Comparing different materials for rotor-can in flooded generators

Wani, Faisal; Dong, Jianning; Yadav, Avinash; Polinder, Henk

DOI
10.1109/ICELMACH.2018.8506730

Publication date
2018

Document Version
Final published version

Published in
Proceedings 2018 XIII International Conference on Electrical Machines (ICEM)

Comparing Different Materials for Rotor-Can in Flooded Generators

F. Wani, J. Dong, A. Yadav and H. Polinder

***Abstract* -- Flooded Generators have been proposed as a possible solution to eliminate the risks due to the seal failure, and improve cooling in tidal stream turbine generators. In a flooded generator, the stator-rotor gap is filled with the seawater; this poses a serious corrosion risk to the material inside the generator. For this reason, a can or a protective shield is used on the stator and the rotor surfaces in the watergap. This paper compares different rotor-can materials based on the eddy current losses in the rotor-can, and its impact on the temperature inside the generator. Due to the flooded gap, the temperature rise in magnets, because of rotor-can eddy current losses is much lower than in a corresponding airgap machine. Thus from the thermal point of view, the choice of the rotor-can material is less critical in a flooded generator than in an airgap generator.**

***Index Terms*-- Tidal stream turbines, Flooded Generators, Permanent Magnets, Rotor-can, Eddy current losses, Demagnetization.**

I. INTRODUCTION

TIDAL energy is predictable, which makes it more favorable than other forms of renewable energy. A typical example of a pod-type (propeller type) tidal stream turbine is shown in Fig. 1. Tidal turbines are submerged in the seawater. Usually, the generators are placed in a sealed enclosure to prevent direct exposure to the corrosive seawater. However, the risk of seal breakdown/deterioration always exists, possibly resulting in the generator failure [1]. To eliminate this failure mode, and improve the overall reliability of the tidal turbine system, a generator capable of operation when the stator-rotor gap is flooded with the seawater has been proposed. Such a generator is commonly known as the Flooded generator. This paper compares different shielding materials in the rotor-can of the flooded generator.

Fig. 2 compares the conventional airgap generator and the flooded generator. As we can see, in direct-drive permanent magnet (PM) flooded generators, protective shields on the rotor and the stator surfaces in the watergap are necessary to prevent the corrosion of the magnets and the failure of the winding insulation, respectively. This protective shielding material should ideally be corrosion resistant, have low electrical and high thermal conductivity, along with strong water-repellent properties. However, it is difficult to find a material which possesses all these properties, and thus a study of different materials becomes necessary.

Fig. 1. An example of a Tidal Stream Turbine: Nova M100 [©Nova Innovation]

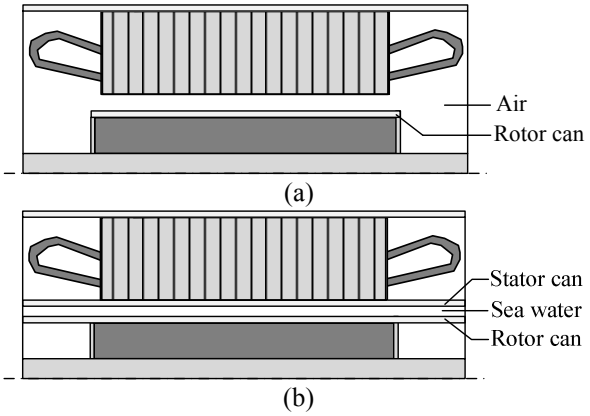

Fig. 2. Sectional view of two types of tidal PM generators: (a) airgap (b) flooded.

Both metallic and non-metallic materials can be used as the protective coating or can. Non-metallic materials such as epoxy, glass fiber reinforced plastic (GFRP), and other carbon fibers have been used in some cases [1],[2]. GFRP could be an excellent candidate for protective coatings as it is non-corrosive and non-conducting, has good fatigue-resistance and can be molded into complex shapes without machining. However, GFRP composites are susceptible to mechanical and electrical failure in the long term due to water ingression [3]. Thus, to provide adequate protection against water ingression, it is usually recommended to use a higher thickness of the GFRP than metallic materials. The thickness of the coating material contributes to the magnetic reluctance, and consequently, influences the volume of magnets required. Magnets being expensive, it is preferable to minimize the coating thickness to keep the overall costs down.

The author has been supported by the TiPA project (Tidal turbine Power take-off Accelerator), which has received funding from the European Union's Horizon 2020 research and innovation programme under grant agreement No 727793, managed by the Innovation and Networks Executive Agency. This paper reflects only the author's view, the Agency is not responsible for any use that may be made of the information the paper contains.

F. Wani and H. Polinder are with Maritime and Transport Technology Department, Delft University of Technology, 2628 CD Delft, Netherlands (email: f.m.wani@tudelft.nl, h.polinder@tudelft.nl).

J. Dong is with Electrical Sustainable Energy Department, Delft University of Technology, Netherlands (e-mail: J.Dong-4@tudelft.nl).

A. Yadav is with Bakker Sliedrecht Electro Industrie B.V., Sliedrecht, Netherlands (e-mail: avinashyadav1301@gmail.com).

978-1-5386-2477-7/18/$31.00 ©2018 IEEE

On the other hand, metallic materials such as non-magnetic steels (e.g. 304L Austenitic Stainless steel), Inconel, and Titanium are used due to their corrosion resistance and excellent waterproofing properties. Furthermore, they may also partially shield magnets from the spatial and the time harmonics of the stator field, thereby, reducing the losses in the magnets. However, these materials add to the overall eddy current losses in the machine [4],[5].

From the above discussion, it is clear that both electrically conductive as well as non-conductive materials maybe used in the protective cans. However, using a conductive material on the stator side causes excessive eddy current losses [6]. Therefore, in this paper we analyze an intermediary design which uses the GFRP coating on the stator side, and a metallic can on the rotor side. As the eddy current losses in the rotor-can are much lower than in a conductive stator-can, smaller thickness of the metallic can over GFRP, might actually minimize the lifetime cost of the generator.

The temperature rise in the magnets resulting from the eddy current losses in the rotor not only reduces their remanent flux density, but may also cause irreversible demagnetization, as shown in Fig. 4. Therefore, the thermal performance of the PM generator must be carefully analyzed while selecting the rotor-can material.

This paper studies different rotor-can materials by comparing the amount of eddy current losses in the rotor-can, and more importantly, its impact on the temperature inside the PM generator, especially the magnets. Both airgap and flooded generator designs are considered, and compared. The main contribution of the paper is to show how different rotor-can materials affect the rotor loss and magnet temperature in different generator configurations. The results provide a valuable guidance to the design of tidal generators.

In the next section, tidal generator design parameters, and different rotor-can materials studied are presented. Section III describes the methodology adopted to calculate the eddy current losses in the PM generator. Section IV briefly highlights the lumped parameter thermal model of the flooded generator. In section V, eddy losses in the rotor-can, and the PM temperature for different rotor-can materials are presented. Conclusions from this paper are given in section VI.

II. System Description

Eddy current losses in the rotor depend on the stator winding layout. PM machines with integer slot windings have negligible losses in the rotor due to the space harmonics. Hence, the choice of the material for the rotor-can is not as critical in these machines [6]. However, same cannot be asserted about the PM machines with fractional slot concentrated windings as they contain significant spatial harmonics in their stator magnetomotive force. For this reason, a fractional slot PM machine with a base winding of 12/10 (slots/poles) is analysed in this paper. This slot-pole combination is frequently used in the design of PM machines.

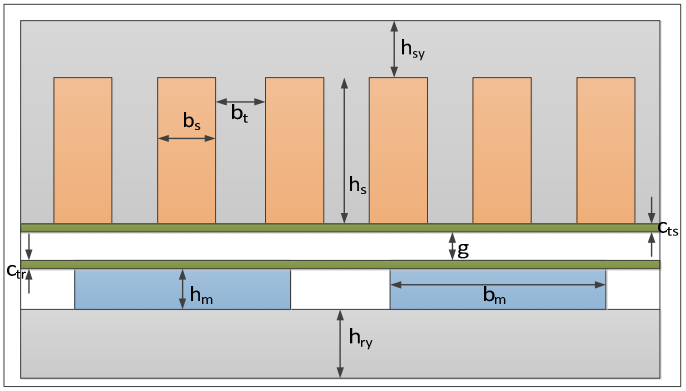

Fig. 3. A part of the 2D cross-section of a Flooded Generator.

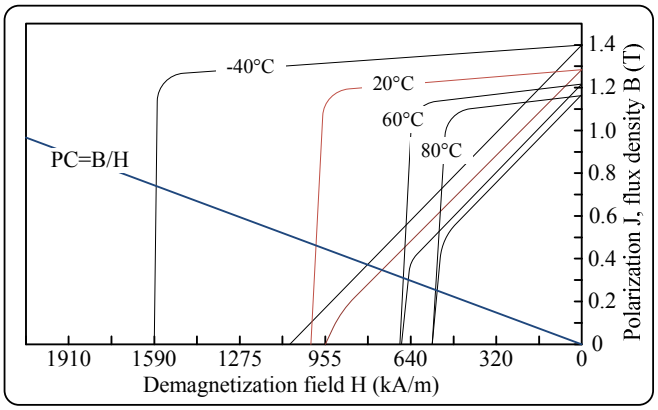

Fig. 4. A typical BH-curve for a NdFeB type permanent magnet.

The dimensions corresponding to the PM generator are listed in Table I. The spatial harmonic spectrum corresponding to this slot-pole combination is depicted in Fig. 5.

Following materials for the rotor-can have been compared:

- Non-magnetic Stainless steel 304L
- Inconel Alloy 718
- Titanium SP 700
- GFRP C-glass

The materials have been chosen as they cover a wide range of thermal and electrical properties, and have been previously considered in Permanent Magnet Canned motors [4]. Obviously, these materials also satisfy the basic criterion of being waterproof and corrosion resistant. Their relevant electrical and thermal properties are given in Table II. As is the case usually, materials with good thermal conductivity also have higher electrical conductivity.

In the case of flooded generator, the water in the stator-rotor gap is not assumed to flow freely in and out of the gap. This is because in most flooded designs, some sort of debris seal would be present to prevent marine life from getting into the watergap, and/or to prevent any loss of material (or fluid) into the ocean from the machine [7].

III. Eddy Current Loss Calculation

A. Assumptions in Eddy current loss model

The rotor eddy current loss calculation method used in this paper is based on the following main assumptions:

- Rotor losses because of the stator slotting are neglected.

- End effects in the rotor can are neglected. Induced currents in the rotor-can and PMs only have axial components.
- Rotor back-iron is assumed to be unsaturated, and laminated. This also implies eddy current losses in the rotor iron are negligible.

For solid rotor iron, the effect of saturation might be substantial. This normally results in higher losses in the back-iron, compared to what has been calculated assuming the linear iron, as the skin depth changes [8]. For the permanent magnets and the rotor-can, saturation in the rotor iron usually means lower losses. In this paper, however, the same assumption of linear rotor iron (with laminations) is applied for the PM generator with different rotor-can materials, without any significant loss of generality.

B. Loss Modelling in the Rotor

Due to the sector symmetry in most electrical machines, modelling a base-winding section is adequate for electromagnetic loss analysis. The same approach has been adopted in this paper. To speed up the eddy current loss calculation model, a linear current density is imposed on the stator bore as a boundary condition, as shown in Fig. 6. This approach has been widely adopted in the literature [8], [9] and simplifies the model significantly.

The linear current density imposed on the stator inner radius is given by [9]:

$$K_s = \frac{3N_{ph}}{\pi R_s}\sum_u I_u \sum_v K_{sov} K_{wv} \sin(up\omega_r t \pm v\theta_s + \theta_u) \qquad (1)$$

where, N_{ph} is the number of turns per stator phase, I_u is the phase current of time harmonic order u (such that $u = 1$ is the fundamental time harmonic) (A), p is the number of pole pairs, ω_r is the rotor speed (rad/s), υ is the space harmonic order (such that $\upsilon = p$ corresponds to the main field). K_{sov} is the slot opening factor, and K_{wv} is the winding factor corresponding to the v^{th} harmonic; R_s is the stator inner radius. The corresponding boundary condition then becomes:

$$n \times H = K_s \qquad (2)$$

where n is the normal at the surface, and H is the magnetic field intensity just inside the boundary. The 2D model is then solved using the finite element analysis. To further simplify and speed up the loss calculation, the linear current density boundary condition is transformed to the rotor frame, using the following transformation in (1):

$$\theta_s = \theta_r + \omega_r t \qquad (3)$$

This simplification gives comparable results to the full 2D cross-section time-stepped transient model for the eddy current loss calculation, whilst minimizing the numerical rigor and time. At all times it must be ensured that the total current in the rotor-can and each magnet segment (individually) adds up to zero. This is achieved by imposing an additional current conservation constraint on each magnet segment:

$$\int J_z \mathrm{d}S_{mag} = 0 \qquad (4)$$

where, J_z is the current density perpendicular to the magnet cross section, and S_{mag} is the cross-sectional area of the magnet.

The eddy current losses in the can and the magnets are then calculated from the following equation:

$$P_{ed} = \int \frac{J_z^2}{\sigma} \mathrm{d}V \qquad (5)$$

TABLE I
DESIGN PARAMETERS FOR PM GENERATOR

Parameter	Symbol	Value
Rated Power	P	300 kW
Rotor speed	ω_m	30 rpm
Remanent density in magnets	B_r	1.25 T
Magnet conductivity	σ_{pm}	5.56e5 S/m
Watergap radius	R_s	1.2 m
Watergap radial length	g	8 mm
Stator can thickness	c_{ts}	3 mm
Rotor can thickness	c_{tr}	2 mm
Magnet-arc to pole-pitch ratio	α_m	0.70
No. of pole-pairs	p	55
No. of slots	Q_s	132
Slot depth	h_s	80 mm
Slot width	b_s	45 mm
Magnet height	h_m	24 mm
Current density in the stator slot	J_s	3e6 A/m^2
Slot fill factor	k_{fil}	0.5
Stack length	l_s	0.7 m
Stator and rotor yoke heights	h_{yoke}	20 mm
Specific hysteresis loss at 1.5 T and 50 Hz	p_{Fe0h}	0.5 W/m^3
Specific eddy current loss at 1.5 T and 50 Hz	p_{Fe0e}	2.0 W/m^3

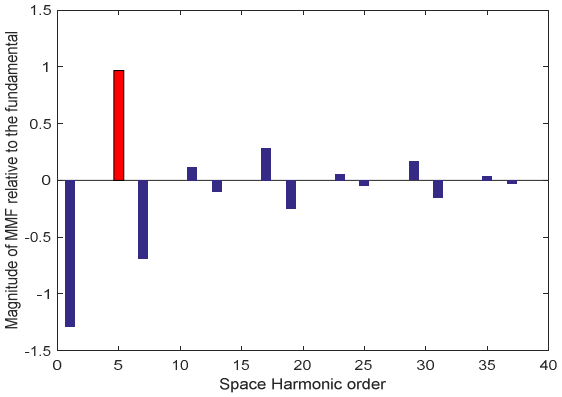

Fig. 5. Three-phase MMF spectrum for Fractional slot concentrated winding (12/10 single layer). Red bar represents the fundamental spatial harmonic.

TABLE II
ELECTRICAL AND THERMAL CONDUCTIVITIES FOR ROTOR-CAN MATERIALS

Material	Electrical Conductivity (MS/m)	Thermal conductivity (W/mK)
Non-magnetic Stainless steel 304L	1.39	16.20
Inconel Alloy 718	0.80	11.40
Titanium SP 700	0.61	7
GFRP C-glass	0	1

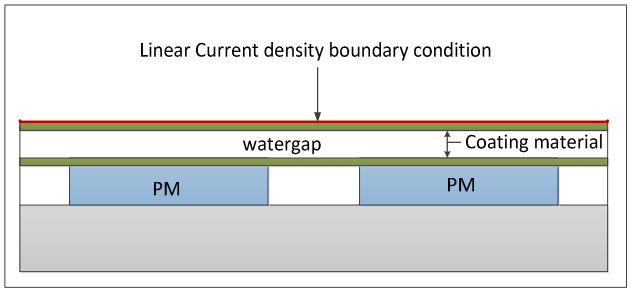

Fig. 6. Calculation of rotor eddy losses by imposing current density on the stator bore.

Where, σ is the electrical conductivity of the material. The integral is evaluated over the volume of the material where the loss occurs. The induced current density itself is calculated from the induced electric field E_z such that:

$$E_z = -\frac{\partial A_z}{\partial t}; \quad J_z = \sigma E_z + J_{ez} \tag{6}$$

where A_z is the magnetic vector potential normal to the 2D modelling plane, and J_{ez} is the circulating current because of the additional current constraint of (4).

C. Iron Loss in the Stator

The total iron loss density in the stator is calculated using the Steinmetz equation [10]:

$$p_{Fe} = 2p_{Fe0h}\left(\frac{f_e}{f_0}\right)\left(\frac{\hat{B}_{Fe}}{\hat{B}_0}\right)^2 + 2p_{Fe0e}\left(\frac{f_e}{f_0}\right)^2\left(\frac{\hat{B}_{Fe}}{\hat{B}_0}\right)^2 \tag{7}$$

where, f_e is the frequency of the field in the iron, $\hat{B}_{Fe}$ is the magnetic flux density in the iron; p_{Fe0h} and p_{Fe0e} are the specific hysteresis and the eddy current losses (W/m^3) at magnetic flux density $\hat{B}_0$ of 1.5 T and frequency, f_0 of 50 Hz.

IV. Lumped Parameter Thermal Model

In this section, the lumped parameter model used in the thermal analysis of the flooded PM generator is briefly outlined. The objective of this analysis is to check the effect of changing the rotor-can material on the magnet temperature, and also on the maximum temperature in the stator slot.

First, a lumped element thermal network is developed for the flooded PM generator. For the airgap generator, modifications are made wherever necessary, such as in the airgap. Various thermal nodes in the machine are connected by means of the thermal resistances, either determined by conduction or by convection, radiation is mostly neglected. However, some empirical convective heat transfer coefficient equations do contain some contribution due to the radiation. Later, some empirical equations are given to estimate the various heat transfer coefficients required to determine the convective thermal resistances in the thermal network model.

The thermal model presented here is based on the following assumptions:

- No axial velocity of water in the flooded gap is assumed. That is, the flow in the watergap is Taylor-Couette.
- Heat flow in the radial and the axial directions are independent of each other.
- No heat flow in the axial direction is assumed in the stator/rotor iron because of the laminated structure.
- No axial heat flow is assumed in the stator-rotor gap as the axial fluid flow is restricted. This is a reasonable assumption to make in direct-drive low speed machines [11]. Under this assumption, the convective heat transfer coefficient is underestimated.

A. Thermal Network

A highly accurate thermal analysis of the electrical machine requires complex finite element analysis and Computational Fluid Dynamics simulations. But for most practical purposes, a lumped element thermal network gives reasonable results, and is a good approach while comparing different designs/materials. An example of the thermal network in the stator slot is shown in Fig. 7.

It should be noted that the nodes which also double as heat sources are modelled using a T-equivalent network; details about the T-equivalent network can be found in multiple references, such as [11], [12]. For the sake of brevity, we do not delve into the details of the thermal model of the PM generator here. References cited above describe thermal modelling of PM machines in detail.

B. Convective Heat Transfer coefficients

When a solid surface is in contact with a fluid, the thermal resistance at the interface is calculated using the heat transfer coefficients. Correct estimation of these heat transfer coefficients is the most difficult task in the thermal modelling of electrical machines. In this paper, however, the focus is not on accurate calculation of the heat transfer coefficients. Here, it suffices to stick with the empirically derived equations to calculate these coefficients.

For a Flooded PM generator, heat transfer coefficients have been used at the following interfaces:

1) *In the Watergap*: In low speed applications, heat flow is mainly radial, if no forced cooling is used. Heat from the rotor is mostly evacuated from the stator housing via the watergap, unless the rotor shaft provides a low resistance path. The heat transfer coefficient in the watergap, α_g is a function of the Nusselt number (*Nu*) such that,

$$\alpha_g = \frac{Nu\lambda}{d_h} \tag{8}$$

where λ is the thermal conductivity of the water in the watergap and d_h is the hydraulic diameter. Nusselt number is a function of the fluid properties as well as the physical dimensions related to the fluid flow. The equations to determine the Nusselt number in (8) are based on the Taylor number, details are mentioned in [11].

2) *Stator House to Ambient Water:* In a pod-type tidal turbine shown in Fig. 1, the velocity of the water on the stator housing surface of the generator is lower than that of the free flow tidal velocity. The heat transfer coefficient at the outer surface increases with the fluid velocity, as convection becomes forced rather than natural. As a conservative approach, we determine the heat transfer coefficient assuming natural convection at the stator housing surface. In any case, this thermal resistance is much lower than the other thermal resistances in the radial direction inside the machine.

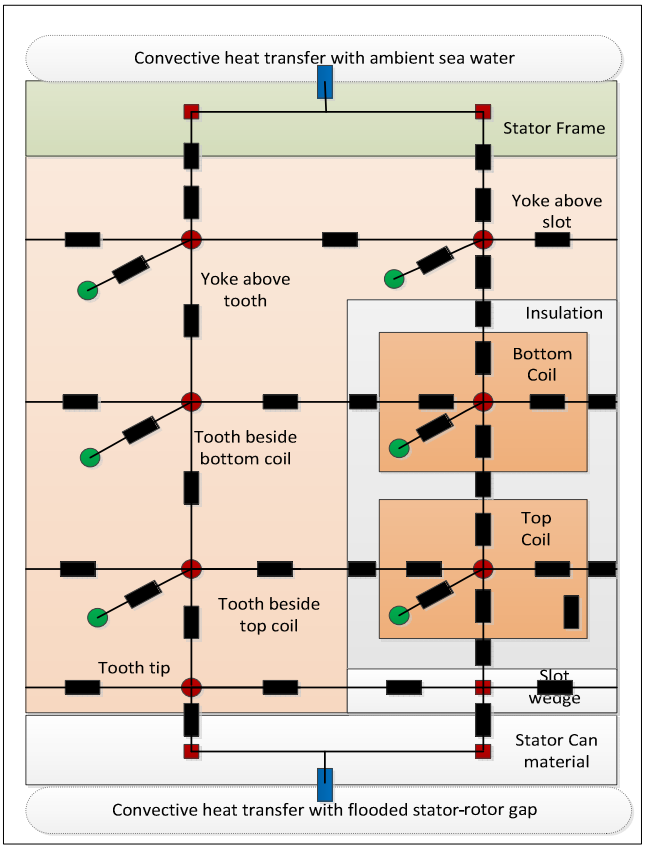

Fig. 7. Lumped element Thermal Network (condensed form) representing the radial flow of heat in the slot of the PM generator with a double-layer winding. This can be modified to accommodate single-layer winding. Green dots represent nodes where heat loss occurs. Black boxes denote thermal resistances due to conduction, whereas blue boxes denote thermal resistances corresponding to the convective heat transfer.

Thus, assuming natural rather than the forced convection does not make significant difference in the temperature estimation inside the machine. The heat transfer coefficient at the outer surface of the stator housing is again found using the Nusselt number as follows:

$$\alpha_{so} = \frac{Nu\lambda}{D_{ext}} \tag{9}$$

where, D_{ext} is the external diameter of the stator housing [13]. The Nusselt number in (9) corresponds to the natural convection rather than the Taylor-Couette flow in (8). Hence, the Nusselt number calculation is slightly different; here, it is calculated from the Grashof and the Prandtl numbers given in [14].

Calculation of the heat transfer coefficients at the end shields to the ambient water interface can be determined using the similar approach. However, the equations for the Grashof and the Prandtl numbers would be different for the end shields. Again, the appropriate equations can be found in any heat transfer textbook, such as [13]. Heat transfer coefficients calculated for the PM generator in this paper are listed in Table III.

3) *End-winding to end-shield:* In a flooded generator, the airflow around the end windings due to the rotor motion is blocked by the protective cans, see Fig. 2(b). Therefore, the heat transfer coefficient near end windings is rather small. For this reason a conservative heat transfer coefficient value of 6 W/m^{2}K has been used. In conventional airgap machines without can, this value is normally between 15-40 W/m^{2}K [12], [15] .

Knowing all these heat transfer coefficients, the thermal resistances R_{th} at the corresponding interfaces, with surface area, A is calculated using the equation:

$$R_{th} = \frac{1}{\alpha A} \tag{10}$$

In the thermal model, an ambient water temperature of 20°C has been assumed. Other parameters used in the thermal model have been listed in Appendix.

V. Results and Discussions

The eddy current losses in the rotor-can and the PMs for different rotor-can materials are listed in Table IV. As an example, the induced eddy current loss density in the stainless steel rotor-can and the magnet is shown in Fig. 8. It is observed that the eddy loss density in the rotor-can is about two orders of magnitude higher than that of the PM. This is because of the higher resistivity of the PM compared to the rotor-can, and also due to the segmented nature of the magnets.

As expected, the eddy losses are the highest in the Stainless steel rotor-can, because of its highest conductivity, see Table IV. Consequently, the magnet temperature corresponding to the stainless steel rotor-can is also higher. This is shown in Fig. 9, along with PM temperatures for other rotor-can materials. Unless the material with very high conductivity is used where shielding effects become substantial, losses will increase with increase in conductivity of the rotor-can.

To assess the impact of the watergap on the magnet temperatures, the watergap was replaced with an equivalent airgap, and then the magnet temperatures were re-evaluated. It was assumed that under both these cases, the losses in the PM generator remained the same. However, in the airgap generator no stator GFRP coating was deemed necessary, and was eliminated from the thermal model, replacing it with an equivalent thickness of the airgap.

It is observed that in the absence of flooding, the temperature rise in the magnets was much higher, as is seen in Fig. 9. Interestingly, a deviation from this trend was observed in the case of the GFRP rotor-can. In other words, when the rotor is covered with a GFRP coating, the magnet temperatures increase rather than dropping by flooding the gap with seawater. This counterintuitive behavior can be explained as follows.

TABLE IIIII
Heat Transfer Coefficients Used in Thermal Network Model of Flooded PM Generator

Interface	**Heat Transfer Coefficient (W/m^{2}K)**
In watergap	570
Stator outer frame to Ambient water	280
End shield to ambient water	60
In the airgap (when watergap is replaced with airgap)	20

TABLE IV
PM and Rotor Can Loss for Different Can Materials

Material	**PM Loss (W)**	**Can loss (W)**
Non-magnetic Stainless steel 304L	601	8660
Inconel Alloy 718	614	5132
Titanium SP 700	617	3939
GRP	622	0

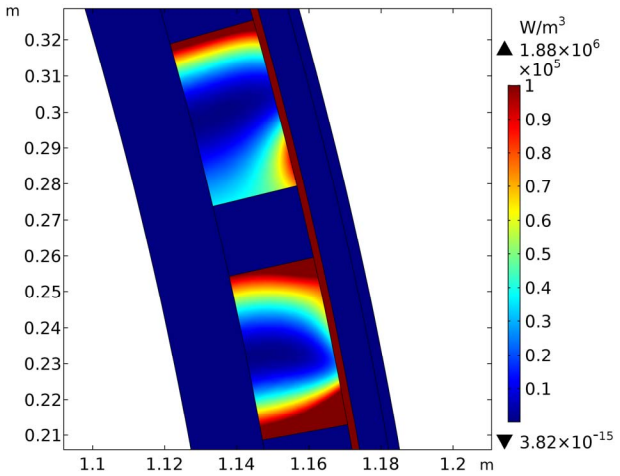

Fig.8. Eddy loss density distribution in the rotor can and a single permanent magnet (Rotor can material: Stainless Steel 304L). FEM simulation software: COMSOL Multiphysics.

On the flooding gap, the heat from the stator is partly evacuated from the rotor as well, resulting in a slight increase of the temperature in the magnets. This is because of the better heat transfer coefficient in the watergap compared to the airgap, see Table III. However, there are other factors also at play here. The amount of heat that will be transferred to the rotor from the stator will also depend on overall thermal resistance from the rotor to the ambient (including bearings and shaft), and the total rotor losses. For instance, if for the same thermal resistances in the rotor, magnet losses were higher, in that case too, the magnet temperature would have dropped upon flooding. This is shown in Fig. 10, where a sensitivity analysis is performed with respect to the magnet conductivity for the GFRP coating. The point of inflection of temperature reversal depends on the total rotor losses and the thermal resistances in the rotor-to-ambient path.

As far as the temperature in the stator slots is concerned, the effect is opposite to that in the magnets, see Fig. 11. That is, in the flooded case, the maximum temperature in the slot is slightly higher than that of the airgap case. Again this is because of the better heat transfer capability of the watergap, which transfers rotor losses more effectively to the stator. As expected, for the GFRP case, where the heat flow from the stator to the rotor, the trend is reversed for the same reason as above.

It is worthwhile to note that while magnet temperatures drop significantly on flooding, the maximum slot temperature increases only slightly. This is because the primary heat evacuation path from the stator slot is via the stator iron- housing-ambient water. Furthermore, in the flooded generator the temperature distribution seems more even, that is, the temperature difference between the slots and the PMs is lower than in a corresponding airgap generator.

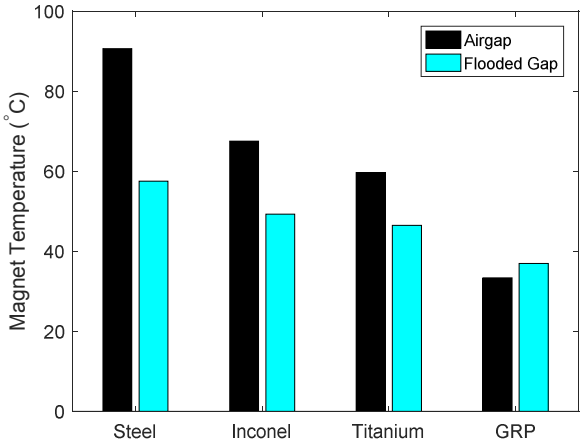

Fig. 9. Temperature inside Permanent Magnet for different rotor-can materials.

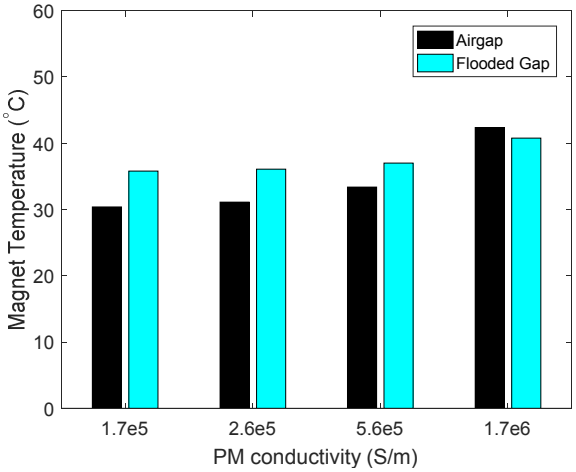

Fig. 10. Temperature of Permanent Magnet for different PM conductivities, under flooded gap and airgap, with GFRP coating on the rotor.

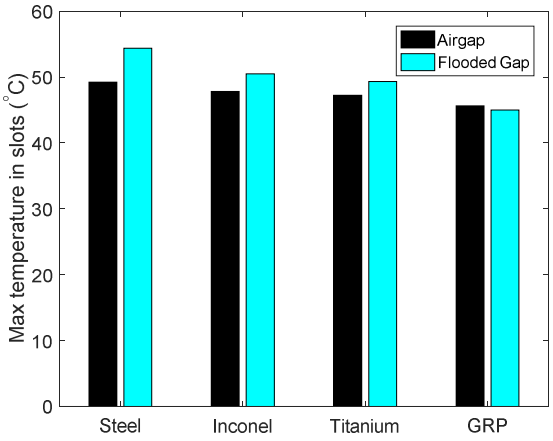

Fig. 11. Maximum Temperature in the stator slots for different rotor can materials. Cooling effect of flooded gap is clearly evident.

Furthermore, the results in this paper are based on the assumption that water in the stator-rotor gap is not exchanged with the seawater. If this is made possible, it is very likely to reduce the temperature of both the stator and the rotor upon flooding. However, it will pose other reliability problems.

Please note that the values given in this section correspond to a particular machine design, which is unlikely to be the 'optimal' design. It is possible to design machines with different dimensions, where the rotor losses can be

minimized with same materials. On the other hand, the conclusions drawn regarding the choice of the materials, and the flooded gap are likely to hold in other designs as well, albeit with different values or points of inflection.

VI. Conclusions

In this paper, different materials for the rotor-can in the flooded generator were compared. Materials with higher conductivity exhibited higher eddy current losses. However, the corresponding temperature rise in the magnets was less than expected because of the flooded stator-rotor gap. In a corresponding airgap machine, the temperature rise in the magnets because of the rotor losses would have been much higher. This means that from the thermal viewpoint, magnets are at a lower risk of demagnetization in a flooded generator.

Our results show that the temperature in the flooded PM generator is more evenly distributed than in a similar airgap PM generator. However, similar analysis must be made for machines of different ratings and sizes, for this conclusion to be generalized. Flooding of the gap might actually increase the temperature inside the stator slots, as more heat from the rotor is evacuated via the stator than from the rotor shaft. Ideally, if sufficient water ingress protection and mechanical robustness is assured over the lifetime of the flooded PM generator, it is better to use materials such as Glass or carbon Fibers as canning materials. Otherwise, a lifetime cost analysis must be carried out with respect to the thickness of the rotor-can material, and the associated eddy losses therein.

VII. Appendix

TABLE V
PARAMETERS USED IN THERMAL MODELLING

Parameter	Value
Thermal conductivity of water	0.7 (W/mK)
Thermal conductivity along the coil	400 (W/mK)
Thermal conductivity through the coil	1.8 (W/mK)
Thermal conductivity of PM	7.6 (W/mK)
Thermal conductivity of insulation	0.2 (W/mK)
Thermal conductivity of iron in the lamination plane	28 (W/mK)
Thermal conductivity of stator housing frame	205 (W/mK)
Frame thickness	10 mm
Air-film contact thickness between stator frame and stator yoke	0.0015 mm

VIII. References

[1] L. Drouen, J. F. Charpentier, E. Semail, and S. Clenet, "Study of an innovative electrical machine fitted to marine current turbines," in OCEANS 2007-Europe, pp. 1–6, IEEE 2007.

[2] O. Krovel, R. Nilssen, S. Skaar, E. Lovli, and N. Sandoy, "Design of an Integrated 100kW Permanent Magnet Synchronous Machine in a Prototype Thruster for Ship Propulsion," in *Proceedings of ICEM*, 2004.

[3] L. Bian, J. Xiao, J. Zeng, and S. Xing, "Effects of seawater immersion on water absorption and mechanical properties of GFRP composites," *Journal of Composite Materials*, vol. 46, pp. 3151-3162, 2012.

[4] Y. Burkhardt, G. Huth, and S. Urschel, "Eddy current losses in PM canned motors," *19th International Conference of Electrical Machines, pp. 1-7,* 2010.

[5] Q. Yu, X. Wang, and Y. Cheng, "Electromagnetic Calculation and Characteristic Analysis of Can Effect of a Canned Permanent Magnet Motor," *IEEE Trans. Magnetics*, vol. 52, pp. 1-6, 2016.

[6] A. Yadav, "Finding Suitable Material for the Retaining Sleeves in Tidal Generators," *Master Thesis*, Delft University of Technology, Netherlands, 2017.

[7] B. Holstein and N. Perner, "Submersible Power Generating Plant, Driven by a Water Flow," *United States Patent*, US 8,410,626, Apr. 2013.

[8] N. Bianchi, D. Durello, and A. Fasolo, "Relationship Between Rotor Losses and Size of Permanent-Magnet Machines," *IEEE Trans. Industrial Applications*, vol. 49, no. 5, pp. 2015–2023, 2013.

[9] Z. Q. Zhu, K. Ng and N. Schofield and D. Howe, "Improved analytical modelling of rotor eddy current loss in brushless machines equipped with surface- mounted permanent magnets," *IEE Proceedings-Electric Power Applications*, vol. 151, no. 6, pp. 641–650, 2003.

[10] H. Li, Z. Chen, and H. Polinder, "Optimization of multibrid permanent-magnet wind generator systems," *IEEE Trans. Energy Conversion.*, vol. 24, no. 1, pp. 82–92, 2009.

[11] J. Nerg, M. Rilla and J. Pyrhonnen, "Thermal Analysis of Radial-Flux Electrical Machines With a High Power Density," *IEEE Trans. Industrial Electronics*, vol. 55, no. 10, pp. 3543–3554, 2008.

[12] A. Grauers, "Design of Direct Driven Permanent Magnet Generators for Wind Turbines," *PhD Dissertation*, Chalmers University of Technology, 1996.

[13] Y. A. Cengel and A. J. Ghajar, *Heat and Mass Transfer, Fundamentals & Application, Fifth Edition in SI Units*, vol. 5, New Delhi: Tata McGraw-Hill, 2015.

[14] D. Staton and A. Cavagnino, "Convection heat transfer and flow calculations suitable for electric machines thermal models," *IEEE Trans. Industrial Electronics*, vol. 55, no. 10, pp. 3509–3516, 2008.

[15] A. Boglietti, A. Cavagnino, D. Staton, M. Shanel, M. Mueller, and C. Mejuto, "Evolution and Modern Approaches for Thermal Analysis of Electrical Machines," *IEEE Trans. Industrial Electronics*, vol. 56, no. 3, pp. 871–882, 2009.

IX. Biographies

Faisal Wani holds MSc degree in Electrical engineering (2016) from Delft University of Technology, Netherlands, and an MSc degree in Wind Technology (2016) NTNU, Norway. Wani is currently a PhD candidate at Delft University of Technology. His research areas include tidal and wind energy conversion systems, with emphasis on electrical machine modelling and reliability of electrical drives.

Jianning Dong received the B.S. and Ph.D. degrees in electrical engineering from Southeast University, Nanjing, China, in 2010 and 2015, respectively. He worked as a post-doc research fellow at McMaster Automotive Resource Centre (MARC), McMaster University, Hamilton, Ontario, Canada. He is now an Assistant Professor at the Delft University of Technology. His main research interests are design, modelling and control of electromechanical systems.

Avinash Yadav received his M.Sc. degree in Electrical engineering from Delft University of Technology, Netherlands in 2017.

Henk Polinder holds a PhD (1998) in electrical engineering from Delft University of Technology, the Netherlands. Since 1996, he has been an assistant or associate professor at Delft University of Technology in the field of electrical machines and drives. He worked part-time at Lagerwey (1998/99), at Philips (2001) and at ABB Corporate Research (2008). He was a visiting scholar at the universities of Newcastle-upon-Tyne (2002), Quebec (2004), Edinburgh (2006) and Itajuba (2014). His main research interests are electric drives for renewable energy (power take off systems in ocean energy, drive trains for wind energy) and maritime applications. He (co) authored over 250 papers.